Since January 2020 Elsevier has created a COVID-19 resource centre with free information in English and Mandarin on the novel coronavirus COVID-19. The COVID-19 resource centre is hosted on Elsevier Connect, the company's public news and information website.

Journal of Controlled Release 341 (2022) 702–715

Contents lists available at ScienceDirect

Journal of Controlled Release

journal homepage: www.elsevier.com/locate/jconrel

RBC-hitchhiking chitosan nanoparticles loading methylprednisolone for lung-targeting delivery

Yaning Ding [a,b], Bai Lv [b,d], Jinpeng Zheng [b], Caihong Lu [b], Jingzhou Liu [b], Yaran Lei [a,b], Meiyan Yang [b], Yuli Wang [b], Zhiping Li [b], Yang Yang [b], Wei Gong [b,*], Jing Han [c,*], Chunsheng Gao [a,b,**]

[a] School of Pharmaceutical Engineering, Shenyang Pharmaceutical University, Shenyang 110017, China
[b] State key Laboratory of Toxicology and Medical Countermeasures, Beijing Institute of Pharmacology and Toxicology, Beijing 100850, China
[c] Faculty of Functional Food and Wine, Shenyang Pharmaceutical University, Shenyang 110016, China
[d] School of Pharmacy, Qiqihar Medical University, Qiqihar 161006, China

ARTICLE INFO

Keywords:
RBC-hitchhiking
Chitosan nanoparticle
Methylprednisolone sodium succinate
Cytokine storm syndrome
Acute lung injury

ABSTRACT

Hyper-inflammation associated with cytokine storm syndrome causes high mortality in patients with COVID-19. Glucocorticoids, such as methylprednisolone sodium succinate (MPSS), effectively inhibit this inflammatory response. However, frequent and chronic administration of glucocorticoids at high doses leads to hormone dependence and serious side effects. The aim of the present study was to combine nanoparticles with erythrocytes for the targeted delivery of MPSS to the lungs. Chitosan nanoparticles loading MPSS (MPSS-CSNPs) were prepared and adsorbed on the surface of red blood cells (RBC-MPSS-CSNPs) by non-covalent interaction. *In vivo* pharmacokinetic study indicated that RBC-hitchhiking could significantly reduce the plasma concentration of the drug and prolong the circulation time. The mean residence time (MRT) and area under the curve (AUC) of the RBC-MPSS-CSNPs group were significantly higher than those of the MPSS-CSNPs group and the MPSS injection group. Moreover, *in vivo* imaging and tissue distribution indicated that RBC-hitchhiking facilitated the accumulation of nanoparticles loading fluorescein in the lung, preventing uptake of these nanoparticles by the liver. Furthermore, compared with the MPSS-CSNPs and MPSS treatment groups, treatment with RBC-MPSS-CSNPs considerably inhibited the production of inflammatory cytokines such as TNF-α and IL-6, and consequently attenuated lung injury induced by lipopolysaccharide in rats. Therefore, RBC-hitchhiking is a potentially effective strategy for the delivery of nanoparticles to the lungs for the treatment of acute lung injury and acute respiratory distress syndrome.

1. Introduction

Cytokine storm/cytokine storm syndrome (CSS) involves generation of an excessive stress response by immune cells to exotically harmful substances and pathogenic microorganisms. These cells release pro-inflammatory cytokines such as interferon (IFN), interleukin (IL), and tumor necrosis factor (TNF), further aggravating tissue inflammation and organ failure [1–4]. Indeed, the body tends to quickly remove these harmful substances or pathogenic microorganisms, thereby inducing an uncontrollable cascade reaction. This results in an imbalance in the immune regulatory system due to the lack of negative feedback and continuous expansion of positive feedback. This effect, in turn, inevitably induces disproportionate increase in the levels of various cytokines, eventually leading to single or multiple organ damage, functional failure, and death [5]. Cytokine storm, a deadly immune phenomenon, is one of the major mechanisms contributing to acute lung injury/acute respiratory distress syndrome (ALI/ARDS) and disease development [6–8].

After SARS-CoV and MERS-CoV, SARS-CoV-2 is the third coronavirus currently causing the coronavirus disease 2019 (COVID-19), an emerging severe respiratory infectious disease in humans [9]. COVID-19-associated pneumonia can induce an exaggerated cytokine storm in the lungs by releasing excessive inflammatory factors, leading to ARDS [2,5,10]. CSS occurs in 10–20% of patients with COVID-19 and is

* Corresponding authors.
** Corresponding author at: School of Pharmaceutical Engineering, Shenyang Pharmaceutical University, Shenyang 110017, China.
E-mail addresses: usnitro2004@126.com (W. Gong), hj-8080@163.com (J. Han), gaocs@bmi.ac.cn (C. Gao).

https://doi.org/10.1016/j.jconrel.2021.12.018
Received 2 September 2021; Received in revised form 24 November 2021; Accepted 15 December 2021
Available online 18 December 2021

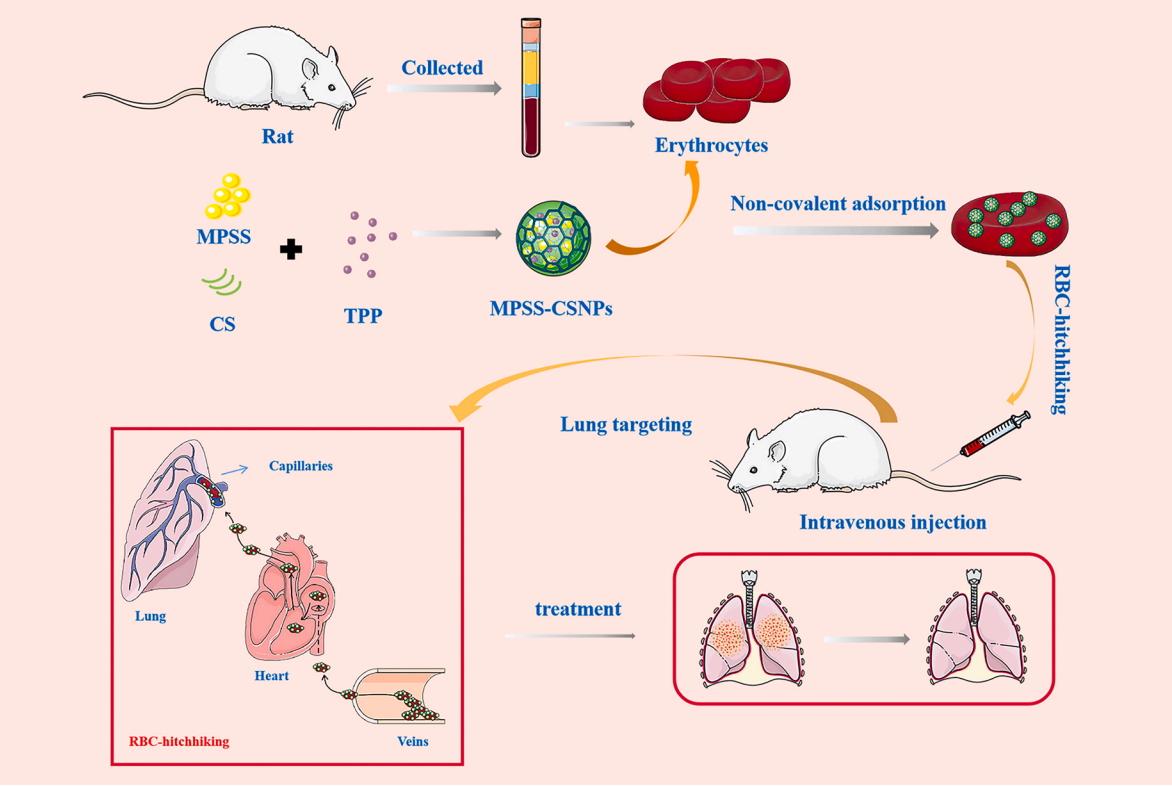

Fig. 1. The study involves preparation of chitosan nanoparticles using the ionotropic-gelation method, which were attached noncovalently to the erythrocytes obtained by centrifugation of the whole blood collected through the abdominal aorta of rats. RBC-hitchhiking facilitated delivery of the chitosan nanoparticles to the lungs to treat inflammation.

associated with significant mortality [11]. The main pathological features are exudation, hemorrhage, epithelial injury, and infiltration of inflammatory cytokines into the lungs. CSS has been reported in patients with severe COVID-19 and having elevated levels of clinical inflammatory markers and increased serum cytokine and chemokine levels, including IL-6, TNF-α and IL-1β [5]. There is no specific treatment for COVID-19; anti-inflammatory intervention may be necessary to prevent acute lung injury in SARS-CoV-2 infection [12]. Glucocorticoids have been widely used in clinics due to their anti-inflammatory and immunomodulatory effects [7,13].

The use of the synthetic glucocorticoid methylprednisolone sodium succinate (MPSS) for non-specific inhibition of the inflammatory response in ARDS has proven to be effective in reducing cytokine storms [14,15]. However, numerous studies have demonstrated that the frequent and chronic administration of glucocorticoids at high doses frequently leads to hormone dependence and serious side effects such as double infections, diabetes, hypertension, and osteonecrosis [16]. Therefore, the development of an effective way to deliver glucocorticoids to the lungs to promote their accumulation in the target organ is of utmost importance. This targeted delivery could allow a reduction in the dose of glucocorticoids and serve as a safe and effective treatment for ALI/ARDS, including COVID-19, or other infectious pulmonary inflammatory diseases.

For the past five decades, nanoparticle-based drug delivery has been used to target specific organs [17–19]. Theoretically, nanoparticles (NPs) provide more advantages than free drugs, including the ability to target any organ while avoiding off-targets, and controlled and sustained release of the drug; these effects improve the therapeutic efficacy of the drugs and reduce their side effects [20,21]. Unfortunately, NPs are rapidly cleared from the bloodstream by the reticuloendothelial system (RES), principally located in the liver and spleen, thereby limiting the dose available at the disease site and considerably reducing the bioavailability of NPs [22]. Erythrocytes (Red blood cells, RBCs) are the most abundant blood components with a longer life span than that of the other blood cells. They can work as carriers for the delivery of a wide variety of therapeutic agents, promoting drug biodistribution, pharmacokinetics, pharmacodynamics, and controlled release [23]. RBC-hitchhiking is a universal drug delivery system solution for dominant liver uptake and limited deposition of nanocarriers in the target organs [24–27]. NPs can be attached to the surface of erythrocytes by non-covalent bonds; thus, the use of RBCs extends the circulation time of NPs and allows targeted accumulation in endothelium-rich organs such as the lungs [28]. Previous studies demonstrated that RBC-hitchhiking improved targeting of the lungs while avoiding the liver and spleen, with a lung-targeting ability approximately fourteen times higher than that of anti-PECAM antibodies, which are in clinical practice for more than 20 years [29].

Chitosan (CS) is a naturally occurring amino-polysaccharide that is widely used in pharmaceutics due to its excellent biocompatibility and biodegradability [30]. The positively charged CS NPs (CSNPs) can be tightly bound to RBCs [31]. Therefore, in this study, RBC-hitchhiking CSNPs loading MPSS (RBC-MPSS-CSNPs) were designed to prolong the retention and duration of action of this drug along with transient accumulation in the lungs while avoiding their uptake by the liver and spleen (Fig. 1). CSNPs loading MPSS (MPSS-CSNPs) were prepared using the ionotropic gelation method and rapidly adsorbed on RBCs *via* electrostatic interaction. The *in vivo* circulation and biodistribution of RBC-MPSS-CSNPs were evaluated to assess RBC-hitchhiking delivery properties. RBC-MPSS-CSNPs increased drug accumulation in the lungs and had a longer circulation time than that of MPSS-CSNPs alone. This approach provides an effective platform for the targeted delivery of drugs.

2. Material and methods

2.1. Materials and animals

Low/medium molecular weight CS with a deacetylation degree of 85% was purchased from Sigma-Aldrich (St. Louis, MO, USA). Tripolyphosphate (TPP) was purchased from Macklin Inc. (Shanghai, China). MPSS was purchased from Qianyan Biotechnology Co., Ltd. (Shanghai, China). 1,1'-Dioctadecyl-3,3,3′,3′-tetramethylindocarbocyanine perchlorate (DiI), fluorescein isothiocyanate (FITC), BCA assay kit, and Annexin V-FITC/PI kit were purchased from Shanghai Beyotime Bio-technology Co., Ltd. Cy7.5 NHS ester (non-sulfonated) was purchased from Shanghai Yuanye Bio-Technology Co., Ltd. Lipopolysaccharide (LPS), and rat TNF-α and IL-6 ELISA kits were purchased from Solarbio Inc. (Beijing, China). The HPLC solvents were of analytical grade and purchased from Fisher Chemicals (Fair Lawn, NJ, USA). All other chemicals were of analytical grade or high purity grade.

Male Fischer (F344) rats and BALB/C mice were purchased from Beijing Vital River Laboratory Animal Technology Co., Ltd. (Permit number: SCXK (Jing) 2016–0006, Beijing, China) and were maintained under SPF conditions for one week before the study. Water and food were freely available throughout the study period. All animal experiments were performed according to the ethics and protocols approved by the Institutional Animal Care and Use Committee at the Academy of Military Science.

2.2. Preparation of MPSS-CSNPs

MPSS-CSNPs were prepared using the ionotropic gelation technique [32]. Briefly, CS was dissolved in 2% (*v*/v) acid solution to obtain a polymer solution with a mass score of 1.5%. This solution was subsequently stirred overnight at 25 °C, and the pH was adjusted to 4.5–4.7 using 1 M NaOH. The CS solution was passed through a 0.45 μm syringe filter to remove residues of insoluble particles. Then MPSS dissolved in methanol was slowly added drop-wise into the CS solution under continuous stirring at 25 °C. The TPP solution was added drop-wise to a fixed volume of the previous solution, and the obtained solution was subjected to continuous stirring for 40 min to obtain MPSS-CSNPs. The NPs were collected by centrifugation at 20,000 rpm for 30 min (XPN-100/90/80, Beckman). The fluorescence probe FITC and near infra-red fluorescence probe Cy7.5 were grafted on CS and then FITC-labeled MPSS-CSNPs (FITC-MPSS-CSNPs) and Cy7.5-labeled MPSS-CSNPs (Cy7.5-MPSS-CSNPs) were prepared using the same method with the aim of monitoring the RBC-hitchhiking behavior and *in vivo* lung targeting ability [33].

2.3. Characterization of MPSS-CSNPs

Nanoparticle size (hydrodynamic diameter, nm) and surface charge (zeta potential, mV) of MPSS-CSNPs were determined by dynamic light scattering (DLS) (Litesizer 500, Anton Parr, Austria). A small amount of MPSS-CSNPs was diluted to 100 μg/mL (carrier's concentration) with distilled water and dripped on the copper mesh (300 mesh). The solvent was evaporated and stained with 2% phosphomolybdic acid for 1 min. The morphology of MPSS-CSNPs was observed using transmission electron microscopy (TEM) (HITACHI, H-7650, Japan).

2.4. Drug encapsulation efficiency and drug loading content

The MPSS loading content in CSNPs was determined by dissolving MPSS-CSNPs in acetonitrile; the solution was filtered through a 0.45 μm filter, and drug loading content was measured using Waters HPLC system (dual λ absorbance detector 2489, separations module e2695, Waters, USA). The standard curve was obtained using MPSS in acetonitrile/water (45:55, *v*/v), and using solutions ranging from 0.05 to 100 μg/mL. The following equations were used to calculate the encapsulation efficiency (EE %) and drug loading (DL-CSNPs %).

$$\text{EE}\ (\%) = \frac{\text{Total amount of MPSS} - \text{Amount of free MPSS}}{\text{Total amount of MPSS}} \times 100\%$$

$$\text{DL} - \text{CSNPs}\ (\%) = \frac{\text{Total amount of MPSS} - \text{Amount of free MPSS}}{\text{Weight of nanoparticles recovered}} \times 100\%$$

2.5. Drug release profile

The dialysis method was used to study *in vitro* release of MPSS and MPSS-CSNPs. Briefly, dialysis bags (MWCO: 30 kDa) containing 2 mL MPSS solution and MPSS-CSNPs were directly immersed into 50 mL phosphate-buffered saline (PBS; 0.1 M, pH = 7.4) placed in a triangular bottle at 37 °C under stirring at 100 rpm. A sample of 1 mL was collected at certain time intervals, and an equal amount of preheated release medium was added immediately to the collected sample. The concentration of MPSS in the collected samples was determined by HPLC. The cumulative percentage of drug release in the NPs was calculated, and the *in vitro* release curve was drawn.

2.6. Adsorption of MPSS-CSNPs to RBCs

The whole blood was collected from the abdominal aorta of healthy male F344 rats, aged 8–10 weeks and weighing 260–300 g, in heparin-coated tubes. The whole blood was centrifuged for 10 min at 1300 *g* and 4 °C to separate RBCs, which were dissolved in 0.9% normal saline and washed three times by centrifugation for 5 min at 850 *g* and 4 °C. MPSS-CSNPs (1 mg/mL) were dissolved in physiological saline, added to the purified RBCs at a volume ratio of 5:1 (NPs: RBC), and the mixture incubated at 37 °C for 30 min. Then, RBCs were sequentially washed thrice to remove unbound particles by centrifugation for 5 min at 180 *g* and 4 °C.

2.7. Drug loading and binding efficiency

A solution of MPSS-CSNPs was added to RBCs at a desired particle/RBC ratio to determine the adsorption of MPSS-CSNPs per RBC after incubation at 4 °C, 25 °C, and 37 °C for different time periods. Non-adsorbed NPs were removed by centrifugation. The MPSS was evaluated by HPLC. The following equations were used to calculate the loading rate of NPs (LR %) and drug loading (DL_{RBC}).

$$\text{LR}\ (\%) = \frac{\text{Amount of MPSS on RBC}}{\text{Total amount of MPSS}} \times 100\%$$

$$DL_{RBC} = \frac{\text{Amount of MPSS on RBC}}{\text{Volume of RBC}}$$

2.8. Morphological analysis

2.8.1. Scanning electron microscopy (SEM)

RBCs and RBC-MPSS-CSNPs were dehydrated for SEM visualization using a standard fixation protocol. Briefly, RBCs were fixed in 2.5% glutaraldehyde solution. Then, the cells were sequentially transferred from PBS to 10%, 30%, 50%, 70%, 80%, 90%, 95%, and 100% ethanol, with each incubation step lasting for 2 min. A small number of cells was collected and spread on a conductive tape to observe the microscopic morphology. The sample was sprayed with gold using a sputtering ion equipment and observed under SEM (S4800, Hitachi, Japan).

2.8.2. Confocal laser scanning microscopy (CLSM)

The NPs loaded on the surface of RBCs were observed by CLSM (LSM 880, Zeiss, Germany). DiI-tagged RBCs and FITC-tagged CSNPs were incubated for 30 min. The samples were then rinsed three times in PBS and observed by CLSM.

2.8.3. Atomic force microscopy (AFM)

The binding efficiency of RBC-MPSS-CSNPs was investigated using mica sheets cut and cleaved into thin sections (1 × 1 cm), with the internal side being used as a substrate. Aliquots (1"L) of MPSS-CSNPs, RBC, and RBC-MPSS-CSNPs were spread on the substrate and air-dried. Atomic force microscopy (AFM) was performed using Bruker Dimension Icon microscope (Bruker Dimension Icon, Germany). The images were captured in the PeakForce Tapping mode, and the MLCT probe with a 10 nm tip was used.

2.9. Damage of RBCs by NPs

2.9.1. RBC osmotic fragility

The osmotic fragility assay was used to evaluate the resistance of RBCs and RBC-MPSS-CSNPs to hypotonic solutions. A total of 100 μL each of RBCs and RBC-MPSS-CSNPs was dissolved in 1 mL of gradually decreasing sodium chloride solution (0.0–0.9% NaCl), and the two mixtures were incubated at 37 °C for 30 min [34]. Next, they were centrifuged at 1300 *g* for 5 min, and the absorbance of the supernatants was recorded at 540 nm using SpectraMax M2 plate reader (Elx-800; Bio-Tek Instruments, USA). The released hemoglobin was expressed as the percentage of the absorbance of each sample relative to that of a completely lysed sample prepared by diluting the stacked cells with 0% NaCl solution.

2.9.2. Turbulence fragility

The turbulence fragility test was used to evaluate the mechanical strength of the RBC membrane. Five hundred microliters of RBCs and drug-loaded RBCs were dissolved in 10 mL PBS and shaken vigorously in an air shaker at 500 rpm for 6 h. A sample of 0.5 mL was collected every hour and centrifuged at 1300 *g* for 5 min; absorbance of the supernatant was measured at 540 nm. A completely lysed cell suspension determined the released hemoglobin.

2.9.3. Phosphatidylserine (PS) exposure

PS exposure in RBCs and RBC-MPSS-CSNPs was measured according to a flow cytometry procedure based on the binding of Annexin V to PS. Briefly, RBCs and drug-loaded RBCs were suspended in PBS and counted. A total number of 5×10^5 cells was collected and centrifuged at 1300 *g* for 5 min; the supernatant was discarded, and 500 μL binding solution was added by pipetting to the pellet to gently dissolve the cells. Five microliters of Annexin V-FITC was added to each sample and incubated for 10–15 min in the dark at 25 °C. PS exposure was detected by flow cytometry.

2.10. Survival of RBC-MPSS-CSNPs

To determine the life-span of RBCs, autologous RBCs and RBC-MPSS-CSNPs were labeled with biotin and then injected into the rats [35]. Briefly, the RBCs or RBC-MPSS-CSNPs were mixed with NHS-biotin (20 μg/mL) at a ratio of 1:100 and incubated at 37 °C for 1 h. The erythrocyte samples were washed three times with physiological saline solution containing 100 mM glycine, and excess NHS-biotin was removed. The labeled RBCs or labeled RBC-MPSS-CSNPs were then injected intravenously into the caudal vein of the donor animal. Serial blood samples (500 μL) were collected from the orbital plexus vein in heparinized tubes after 5 min, 1 h, 3 h, 5 h, 12 h, 24 h, 3 d, 5 d and 7 d of injection. Next, the erythrocyte samples were diluted with PBS, and 5×10^5 cells were incubated with an appropriate dilution of FITC-labeled streptavidin (Nanjing Xinfan Biological Technology Co., Ltd., Nanjing, China) for 1 h at 37 °C. After removal of excess fluorescent reagent, the relative levels of NHS-biotin-streptavidin-FITC binding on erythrocytes were determined by flow cytometry. The average fluorescence intensity of 10 min was calculated as 100% cell survival rate.

2.11. In vivo pharmacokinetic study

Eight-week-old healthy male F344 rats weighing 250–300 g were randomly divided into three groups ($n = 5$): Free-MPSS, MPSS-CSNPs, and RBC-MPSS-CSNPs, and the corresponding compound was injected into rats at a dose of 12 mg/kg (according to the MPSS content). Five hundred microliters of blood were collected from the fundus venous plexus of the rats at 2 min, 10 min, 30 min, 45 min, 1 h, 2 h, 4 h, 6 h, 8 h, 12 h, 24 h, 36 h, and 48 h after administration, and placed in a centrifuge tube containing heparin sodium. The plasma was separated from the blood, and the cells were isolated as previously described.

The MPSS concentration in the rat plasma was determined using Agilent HPLC electrospray ionization tandem mass spectrometry system (Pump G1312C, Autosampler 1367E, Degasser G1322A, G6460A triple quad mass spectrometer, Agilent Technologies, USA). Verapamil hydrochloride was used as the internal standard (IS). The separation of MPSS from IS was achieved by an automated injection of 5 μL samples into a reversed phase C18 analytical column (Agilent Zorbax SB C18, 2.1 × 100 mm, 3.5 μm, Agilent Technologies, USA) under isocratic conditions of acetonitrile and water with 0.1% (*v*/v) formic acid (40:60, v/v) at a flow rate of 0.3 mL/min.

The triple-quadrupole mass spectrometer was operated in positive ionization mode, and detection and quantification were performed using multiple-reaction monitoring (MRM). Tandem mass spectrometry (MS/MS) detection was conducted by monitoring the fragmentation of 457.1 → 253.1 (*m/z*) for MPSS and 455.2 → 165.1 (m/z) for IS. The product ions were generated using a collision energy of 20 eV and 30 eV for MPSS and IS, respectively. The optimized MS parameters were as follows: fragment voltage, 130 V and 160 V for MPSS and IS, respectively; capillary voltage, 4000 kV; gas temperature, 350 °C; gas flow, 12 L/min; nebulizer pressure, 25 psi.

A volume of 100 μL of plasma was added to 10 μL of IS (10 ng/mL) and 400 μL acetonitrile to precipitate the proteins. After vigorous vortex-mixing for 3 min, the samples were centrifuged at 14,000 rpm for 5 min. Five microliters of the supernatant was injected into the HPLC-MS/MS system.

2.12. In vivo distribution study of MPSS-CSNPs

2.12.1. In vivo biodistribution

FITC-labeled CSNPs were used to study the distribution of RBC-hitchhiking FITC-labeled CSNPs (RBC-FITC-CSNPs) and free FITC-labeled CSNPs (FITC-CSNPs) *in vivo*. Male F344 rats were randomly divided into two groups ($n = 3$): FITC-CSNPs and RBC-FITC-CSNPs. The corresponding compounds at the same dose were intravenously injected into the rat tail vein. Three rats of each group were sacrificed at 2, 4, 8, 12, and 24 h, and their heart, liver, spleen, lung, kidney, and blood were collected. Ten milliliters of PBS was used for cardiac perfusion to prevent NPs in the blood affecting the results. The collected organs were weighed and immersed in 2 mL methanol solution (methanol: HCl = 9:1). These organs were centrifuged for 10 min at 10000 rpm and 4 °C. Two hundred microliters of the supernatant was collected and the fluorescence intensity was determined using a fluorescence microplate reader (ex = 485 nm, em = 528 nm). The FITC content in each tissue and blood at different time points was calculated according to the tissue weight and blood volume. Confocal microscopy was used to confirm the effective tissue distribution.

2.12.2. Small animal imaging

BALB/C mice were used for *in vivo* imaging because this procedure is easier to perform in mice than in rats. Near-infrared Cy7.5 was used instead of FITC to prepare Cy7.5-labeled CSNPs (Cy7.5-CSNPs) for *in vivo* investigation. BALB/C mice aged 7–8 weeks and weighing 25–35 g were randomly divided into two groups ($n = 6$): Cy7.5-CSNPs and RBC-hitchhiking Cy7.5-labeled CSNPs (RBC-Cy7.5-CSNPs). The corresponding compounds were intravenously injected into the mouse tail vein at

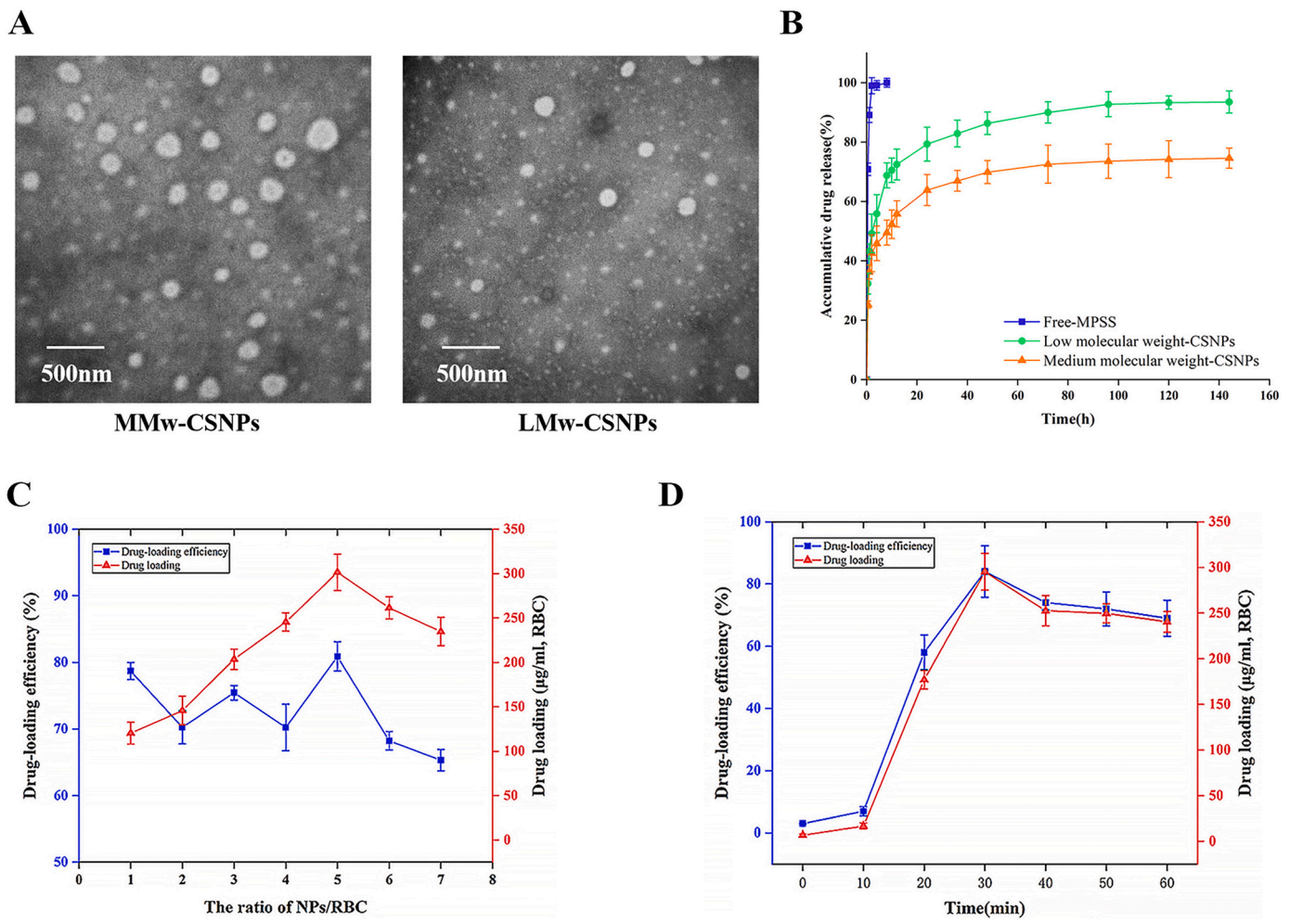

Fig. 2. Transmission electron microscopy (TEM) images of MPSS-CSNPs: MMw-MPSS-CSNPs; LMw-MPSS-CSNPs (A). (B) *In vitro* MPSS release profiles of MPSS injection and MPSS-CSNPs in PBS, pH 7.4. Data represented the mean ± SD ($n = 3$). The effects of (C) the volume ratio of nanoparticles solution to red blood cells (NPs/RBC), and (D) incubation time on the adsorption of nanoparticles to erythrocytes. Data represented the mean ± SD (n = 3). (For interpretation of the references to color in this figure legend, the reader is referred to the web version of this article.)

the same dose. Mice were sacrificed at predetermined time points, and distribution of Cy7.5 was observed using a small animal imaging system (IVISS spectrum type, PerkinElmer limited Company, USA).

2.13. *In vivo therapeutic study*

2.13.1. *LPS-induced ALI rat model*

Eight-week-old male F344 rats were anesthetized by intraperitoneal injection of 5% chloralhydrate in 2.5 mL saline and immobilized on specialized rodent intubation sloping plates. LPS at a dose of 12 mg/kg body weight was dissolved in 400 μL PBS and administered through the trachea to induce acute lung injury. MPSS, MPSS-CSNPs, and RBC-MPSS-CSNPs at the same dose were intravenously injected through the tail vein after 5 h of LPS administration. The blood samples were collected from the eye socket vein of the rats at −5, 0, 2, 4, 6, 8, 12, 24, and 48 h to monitor the progression of the cytokine response. These blood samples were stored overnight at 4 °C, centrifuged at 2500 *g* for 10 min, and the serum was collected for testing. The rats were sacrificed at 48 h to collect the bronchoalveolar lavage fluid (BALF) and samples of the lungs.

2.13.2. *Bronchoalveolar lavage fluid (BALF) collection and lung cytokine evaluation*

The left and right lungs were separated after the rats were sacrificed by surgically ligating the trachea to allow the collection of BALF. BALF was collected three times through the ice-cold PBS instilled up to a total volume of 2.5 mL (BALF could reach ~85%). The collected BALF was centrifuged for 10 min at 1000 *g* and 4 °C. The supernatant of BALF was collected, and the BCA assay kit was used to determine the total protein content. The myeloperoxidase (MPO) level in BALF was quantified using MPO ELISA kit, while an ELISA kit was used to evaluate TNF-α and IL-6 levels. The cell pellets harvested after centrifugation were treated with an RBC lysis buffer to remove RBCs. Afterwards, the remainder of cell suspensions was employed to assess neutrophils (PMNs) level in BALF. Briefly, cells were incubated with PE, Ly-6G and FITC-CD11b for 20 min at 4 °C, then the cells were washed by PBS *via* centrifugation and finally re-suspended in 2% PFA for PMNs determination. The data were analyzed using flow cytometry.

2.13.3. *Lung wet-to-dry weight (W/D) ratio*

A portion of the right lung that was not subjected to lavage was collected and considered as the wet weight; after drying at 50 °C for 48 h, it was reweighed, and this weight was considered as the dry weight. The ratio of lung wet-to-dry weight was calculated.

2.13.4. *Quantitative real-time (qRT)-PCR*

Total RNA of the lung tissue was collected using the Trizol method (BeiJing GenePool Biotechnology Co. Ltd). Then RNA was reverse

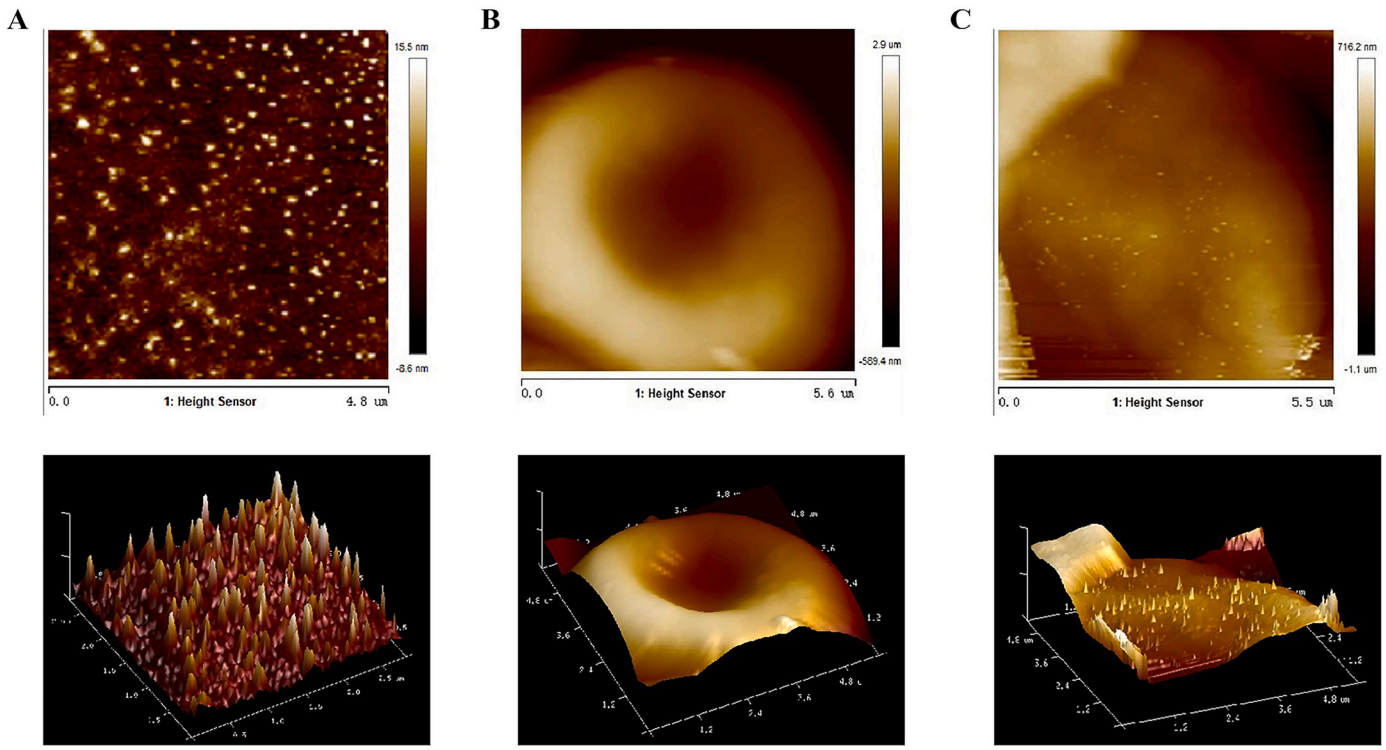

Fig. 3. Atomic force microscopy images of (A) MPSS-CSNPs, (B) RBC and (C) RBC-MPSS-CSNPs. 3D images of (A), (B) and (C).

transcribed into cDNA using a Reverse Transcription Kit (BeiJing GenePool Biotechnology Co. Ltd). The real-time PCR was conducted using the StepOnePlus Real-Time PCR System (Thermo Fisher Scientific, Carlsbad, CA, USA). Twenty-microliter reaction mixtures consisting of 20 ng of cDNA, 10 μL of 2 × SYBR Green (BeiJing GenePool Biotechnology Co. Ltd), 0.8 μL of primers (10 μM) for the target gene, and the internal control. The data were acquired using the Stepone2.3.

2.13.5. Western blot analysis

Western blot analysis was performed as described previously [36]. Briefly, the collected samples of the lung tissues were added in protein lysate. Protein concentrations were determined by the BCA assay kit. Twenty-five micrograms of protein sample was resolved by SDS-PAGE gels and then transferred to PVDF membranes (Millipore Corporation, USA). Transblotted PVDF membranes were blocked with 5% skimmed milk powder (dissolved in TBST, pH 7.5) for 2 h. Subsequently, the membranes were placed in the primary antibody and incubated overnight in a refrigerator at 4 °C. The membrane was washed and incubated with horseradish peroxidase-conjugated anti-rabbit monoclonal secondary antibodies for 40 min. Specific proteins were detected by chemiluminescent western blotting (CAVOY, Beijing, China).

2.13.6. Histopathology and immunohistochemistry

The lung tissue was fixed in 4% paraformaldehyde for 48 h and embedded in paraffin. Four-micrometer-thick paraffin sections were cut, dewaxed in xylene, and dehydrated with gradient alcohol [37]. The sections were stained with hematoxylin and eosin (H&E) for histological analysis. Other sections were used for immunohistochemistry and incubated with 3% catalase for 10 min at 25 °C to block the endogenous catalase. After washing with PBS three times, 5% BSA blocking solution was added to remove BSA, and anti-caspase 1 (protein Tech: 22915–1-ap), or anti-IL-1β antibodies were added (Abcam: ab9722) at a dilution of 1:500 in PBS. The sections were incubated overnight at 4 °C in the dark; then, the secondary antibody was added and incubated for 50 min at 4 °C. The color development was obtained using 3,3′-diaminobenzidine (DAB), and hematoxylin was used for counterstaining. The results were observed under an inverted fluorescence microscope (Japan Nikon Eclipse Ti-SR). The positive rate of immunohistochemistry was analyzed according to the tissue-staining test.

2.14. Statistical analysis

Statistical analysis was performed using the SPSS 23.0 (SPSS Inc., Somers, NY, USA). Statistical analysis of the pharmacokinetic parameters was performed using the *t*-test. Untransformed and log-transformed data for the pharmacokinetic parameters were analyzed using one-way analysis of variance (ANOVA). All values were expressed as mean ± standard deviation, unless otherwise stated. A value of $p < 0.05$ was considered statistically significant.

3. Results and discussion

3.1. Characterization of MPSS-CSNPs

The MPSS-CSNPs were successfully prepared by the ionotropic gelation method using CS of different molecular weights. The TEM experiments confirmed that the MPSS-CSNPs were nearly spherical, with a relatively uniform distribution (Fig. 2A). The mean diameter of the low molecular weight-CSNPs (LMw-MPSS-CSNPs) and medium molecular weight-CSNPs (MMw-MPSS-CSNPs) were approximately 120.6 nm and 233.3 nm, respectively, with positive zeta potential of +14.5 mv and + 30.0 mV, respectively, and narrow particle size distribution (PDI less than 0.2) (Table S1). MPSS-CSNPs prepared using CS of different molecular weights showed a significant difference in diameter and zeta potential. The diameter of MMw-MPSS-CSNPs was significantly higher than that of LMw-MPSS-CSNPs. The moderate-sized NPs showed increased binding efficiency to RBCs than did the smaller NPs [29,31,38]. Moreover, the zeta potential of all MPSS-CSNPs was positive and relatively high, which demonstrated good physicochemical stability of the colloidal suspensions and suggested the possibility of stronger and prolonged interactions with the cells having negative surface charge such as RBCs [31,39].

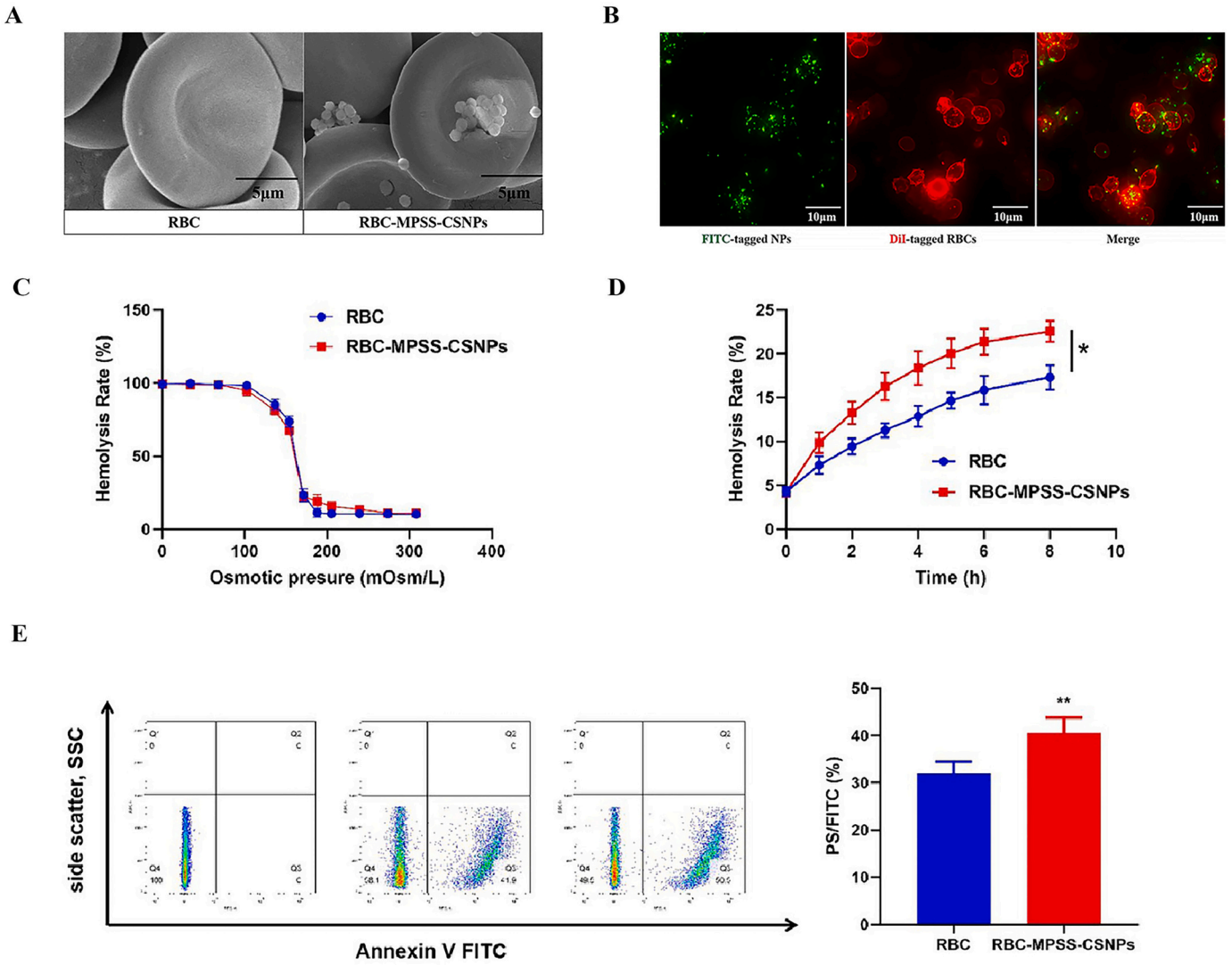

Fig. 4. Scanning electron microscopy (SEM) (A) and confocal laser scanning microscope (CLSM) (B) of RBC-hitchhiking nanoparticles. (C) Osmotic fragility curves and (D) turbulence fragility curves of RBC and RBC-MPSS-CSNPs. PS on the outer surface of RBC and RBC-MPSS-CSNPs. (E) SSC-FITC scatter plot and the rate of PS/FITC. $^{*}p < 0.05$, $^{**}p < 0.01$, represented RBC-MPSS-CSNPs compared with RBC. (mean ± SD, $n = 3$).

MPSS release in PBS (pH 7.4) from free MPSS and MPSS-CSNPs were compared. An amount greater than 90% MPSS was rapidly released within 1 h. The MPSS release rate decreased as the molecular weight of CS increased. The cumulative release of MPSS (%) from LMw-MPSS-CSNPs and MMw-MPSS-CSNPs were 93.52% and 74.58%, respectively (Fig. 2B). In contrast, MPSS-CSNPs showed an initial burst release of the drug within the first hour, reaching a plateau, which is often associated with the release of hydrophilic molecules from the polymeric carriers, after 12 h, followed by a phase of very slow drug release [40]. This could be due to the fact that CS of medium molecular weight possesses higher viscosity of the outer shell of the drug-loaded particles upon contact with the dissolution medium than that of CS of low molecular weight [39,41]. Because of better sustained-release effect and larger size and zeta potential than those of the LMw-MPSS-CSNPs, the MMw-MPSS-CSNPs were selected for our subsequent experiments.

3.2. MPSS-CSNPs binding to RBCs in vitro

Nanoparticles prepared with various materials (such as poly (lactic-*co*-glycolic acid), polystyrenesulfonate, and CS) could be adsorbed on the surface of RBCs [19,24,25]. The interaction forces between NPs and RBCs were mainly electrostatic and hydrophobic. Positively charged CSNPs were mainly adsorbed on the surface of negatively charged RBCs by electrostatic interaction.

The influence of the incubation time and the volume ratio of NPs to RBCs (NPs/RBCs) on adsorption efficiency was examined by drug loading and loading rate of the NPs [23]. The drug loading and loading rate of the NPs increased at first and then decreased. The ratio of NPs/RBCs was set at 5:1 to achieve a high drug loading and loading rate of the NPs (Fig. 2C). Positively charged NPs possess a faster adsorption rate to RBCs than that of negatively charged NPs; accordingly, an incubation time of 30 min was sufficient to achieve the maximum drug loading and loading rate of the NPs (Fig. 2D).

The AFM and SEM showed that the spherical NPs were absorbed on the surface of the RBCs (Figs. 3 and 4A). The CLSM also revealed that a large number of green fluorescent NPs were adsorbed on the surface of RBCs (Fig. 3C). The RBC-MPSS-CSNPs retained the shape of a biconcave disk, similar to the shape of natural RBCs.

A previous study showed that the adsorption of NPs in high loadings can have detrimental effects on RBCs [21]. The damaged RBCs may be destroyed and eliminated quickly from the circulation by macrophages, leading to a reduced targeting ability and circulation performance *in vivo* [28,31,42]. Therefore, the turbulence fragility, osmotic fragility, and PS exposure at the cell surface of RBCs were evaluated after NPs were

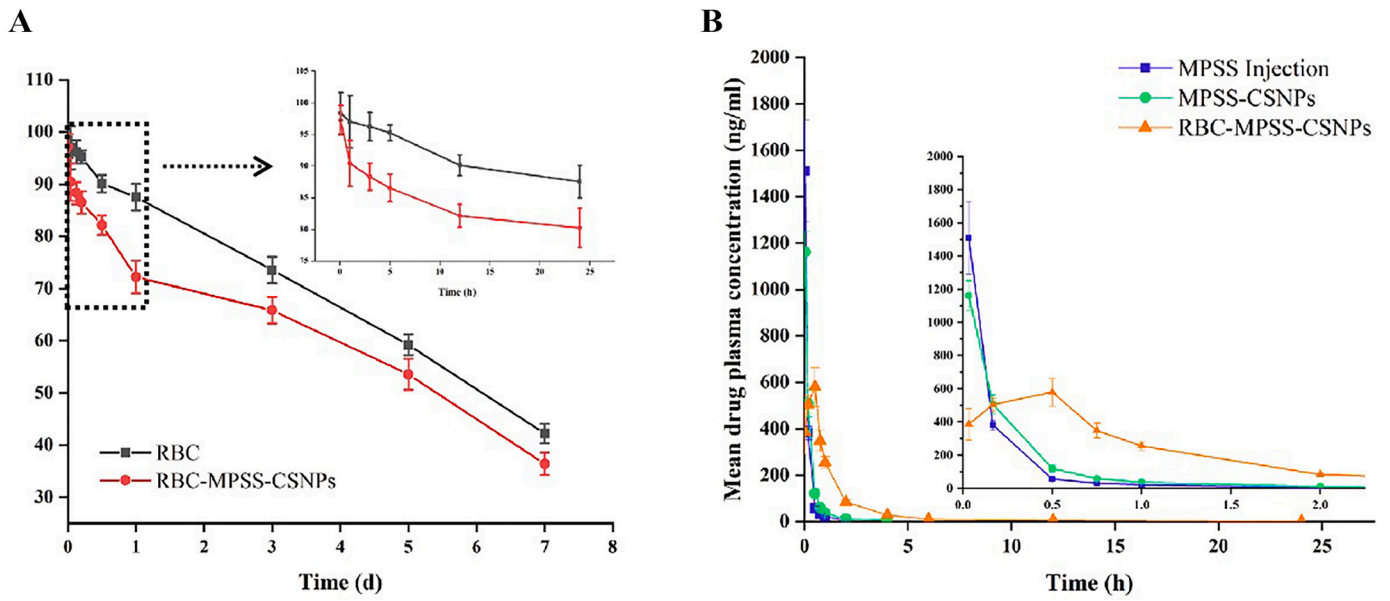

Fig. 5. (A) *In vivo* survival of RBC and RBC-MPSS-CSNPs. Data are represented as mean ± SD ($n = 5$). (B) Mean plasma concentration of MPSS *versus* time follow single dose intravenous administration of MPSS injection, MPSS-CSNPs and RBC-MPSS-CSNPs in rats. The data are presented as the mean ± SD (n = 5).

adsorbed on the surface of RBCs. The hemolysis rate of RBC-MPSS-CSNPs was not significantly different from that of RBCs in a hypotonic solution (Fig. 4A). The results of turbulence fragility revealed that the release of hemoglobin from RBC-MPSS-CSNPs was markedly higher than that of RBCs under shock conditions (Fig. 4B).

Early apoptosis is characterized by PS translocation from the inner to the outer layer of the plasma membrane, and membrane damage is evaluated by measuring the binding of Annexin V-FITC to the exposed PS. The results showed that the PS in the outer layer of RBC-MPSS-CSNPs was significantly more abundant than that in the outer layer of RBCs, indicating that the adsorption of NPs might have caused some damage to RBCs (Fig. 4C).

The damage of RBCs caused by the adsorption and preparation process of NPs is inevitable. Controlling the important influencing parameters, including the proportion of NPs/RBCs and reducing the shear stress damage in the preparation process, could control damage such as red blood cell hemolysis, but only to a minimal extent [40,41]. However, damage of carrier RBCs, drug delivery function, and side effects were acceptable as long as they did not significantly shorten the life of carrier RBCs and affect the drug delivery function.

3.3. Survival of RBC-MPSS-CSNPs

To study the *in vivo* circulation time of RBC-MPSS-CSNPs, FITC-labeled streptavidin tracking of biotin-labeled erythrocytes was used to observe the cycling time of RBC or RBC-MPSS-CSNPs *in vivo*. As shown in Fig. 4, the survival rates of both RBCs and RBC-MPSS-CSNPs in rats gradually decreased with time. The survival rate of erythrocytes adsorbed with NPs was significantly lower than that of free erythrocytes. This suggests that the adsorption and preparation process of NPs might have caused some degree of damage to erythrocytes. The damaged erythrocytes were removed after entering the body circulation. However, 71.85 ± 3.21% of the erythrocytes in the RBC-MPSS-CSNPs group survived after 24 h of circulation *in vivo* and 36.42 ± 2.14% after 7 d of reinfusion. Considering the effect of sampling and fluorescence attenuation, these damages were acceptable and did not significantly shorten the life span of carrier RBCs and affect the drug delivery function. Moreover, carrier RBCs accounted for only a small part of the total number of RBCs in the donor. The damaged carrier RBCs may have a shorter life span than normal RBCs, but they can be phagocytized and cleared similar to other abnormal RBCs in the body, and therefore will not cause adverse effects in the donor.

3.4. In vivo pharmacokinetic study

The mean plasma concentrations of MPSS *versus* time after single doses of MPSS injection, MPSS-CSNPs, and RBC-MPSS-CSNPs were administered to the rats are shown in Fig. 5. The pharmacokinetic parameters are summarized in (Table S2). The half-life of MPSS-CSNPs was significantly longer than that of MPSS ($^{*}p < 0.05$). The mean residence time (MRT) of MPSS-CSNPs was also significantly longer than that of MPSS ($^{**}p < 0.01$). This indicated that MPSS-CSNPs significantly prolonged the circulation time of MPSS, as expected. Initially, MPSS plasma concentration after administration of MPSS injection and MPSS-CSNPs were high (more than 1 μg/mL). However, MPSS concentration decreased rapidly and non-detectable after 2–4 h of administration. However, the rate of decrease of drug concentration in the RBC-MPSS-CSNPs group was significantly lower than that of the MPSS injection group and MPSS-CSNPs group. Although the maximum concentration of MPSS in the RBC-MPSS-CSNPs group was significantly lower than those of the two groups, MPSS was detected up to 24 h. Notably, the mean residence time (MRT) of the RBC-MPSS-CSNPs group was remarkably higher than those of the other groups. Moreover, the area under the curve (AUC) of RBC-MPSS-CSNPs group was 861.85 ng/mL·h, which was significantly higher than that of the MPSS-CSNPs group (334.32 ng/mL·h) and the MPSS injection group (281.78 ng/mL·h). The half-life of MPSS was approximately 0.5 h; therefore, the drug was unmeasurable shortly after the administration of MPSS injection [43,44].

The NPs can have prolonged circulation time, but the clearance performed by the RES results in rapid removal of NPs from the circulation [45]. In contrast, RBC-hitchhiking could dramatically prolong the circulation time of NPs, potentially due to reduced RES clearance [24,31,46]. Moreover, the prolonged circulation time of the RBC-MPSS-CSNPs could extend the duration of action of the drug and improve its bioavailability. On the other hand, the prolonged circulation time of the RBC-MPSS-CSNPs might contribute to desorption of NPs from RBCs and accumulation in the lungs.

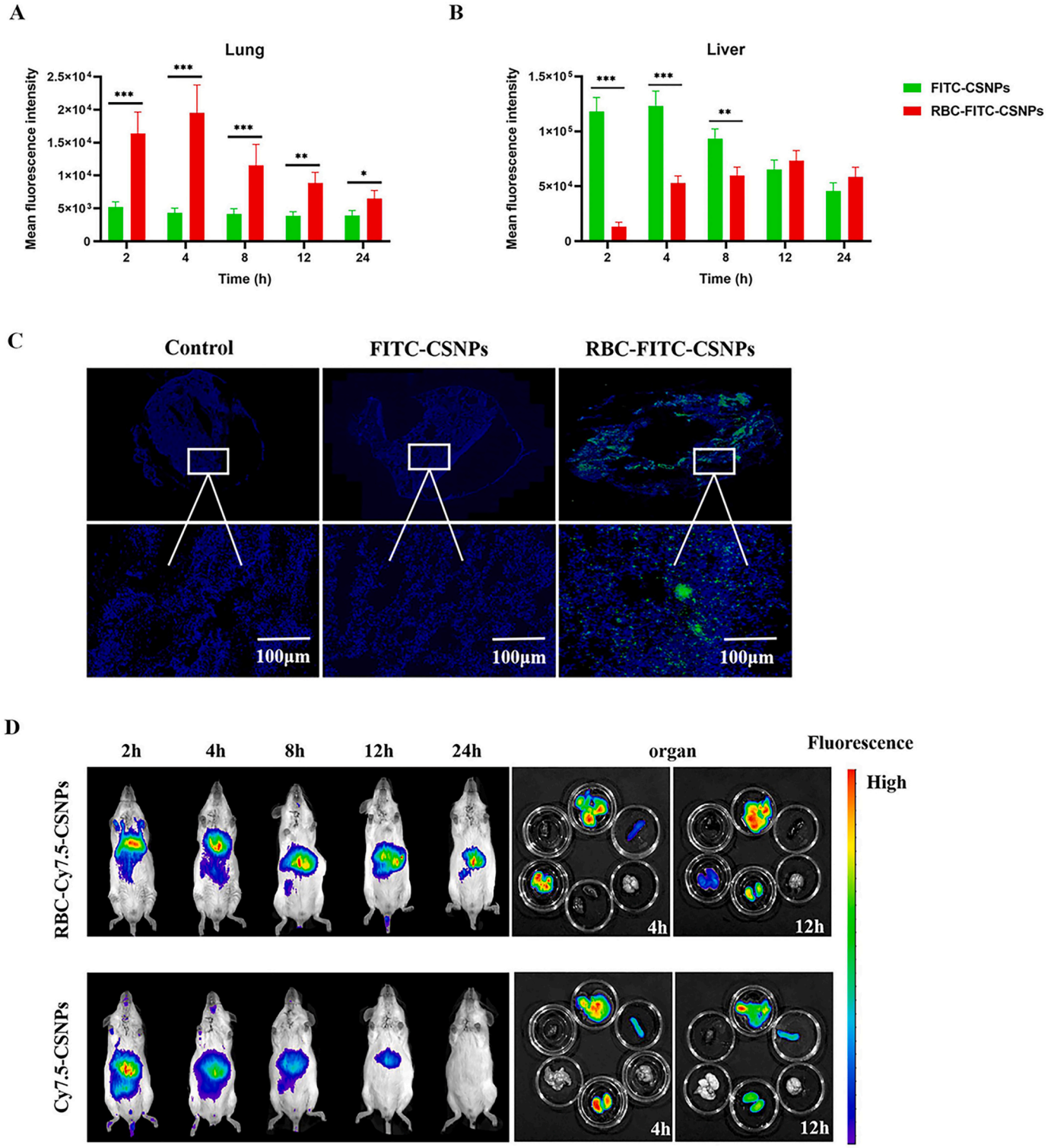

Fig. 6. *In vivo* biodistribution analyses. The distribution of fluorescence of FITC in the lung (A) and liver (B) after injected FITC-CSNPs and RBC-FITC-CSNPs, respectively. All data represent mean ± SD ($n = 3$). $^{*}p < 0.05$, $^{**}p < 0.01$, $^{***}p < 0.001$, compared with infected rat with FITC-CSNPs. (B) Rats were injected with FITC-CSNPs and RBC-FITC-CSNPs, sacrificed four hours later, and then the lungs were fixed and sectioned. Thick white lines represent scale bars of 100 μm. (C) Cy7.5-CSNPs and RBC-Cy7.5-CSNPs were intravenously injected into rat and monitored at specific time points. The mice were sacrificed at 4, 12 h and dissected for liver, heart, lung, kidney, brain, spleen and lung. (In terms of top to bottom and left to right in the last image). All data represent mean ± SD ($n = 6$).

3.5. *Feasibility of RBC-hitchhiking lung-targeting delivery*

In addition to the prolonged circulation of NPs, several studies showed that RBC-MPSS-CSNPs reduced RES uptake and resulted in the accumulation of RBC-MPSS-CSNPs in high amount in the lungs [24,47,48]. The luciferase signal in the rat's lungs and liver (Fig. 6A and B) showed that the pulmonary fluorescence intensity in the RBC-FITC-CSNPs group was the highest post injection and was significantly higher than that of the FITC-CSNPs group. The lung tissue sections observed by fluorescence microscopy (Fig. 6C) revealed high intensity of

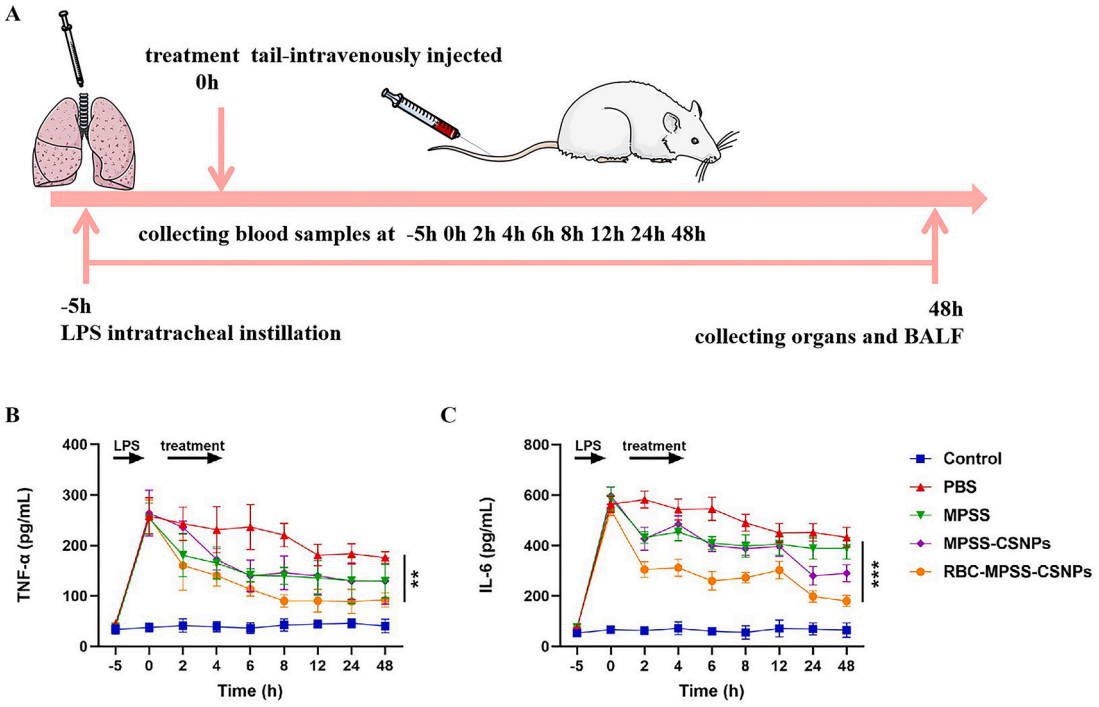

Fig. 7. (A) Schematic illustration of treatment regimens. Levels of inflammatory cytokines in blood of rats infected with pneumonia. (B)TNF-α and (C) IL-6 in blood of rats treated with PBS, inject MPSS, MPSS-CSNPs and RBC-MPSS-CSNPs. Data represent mean ± SD ($n = 6$). $^{**}p < 0.01$, $^{***}p < 0.001$ *vs* PBS.

green fluorescence in the lungs when treated with RBC-FITC-CSNPs, whereas the fluorescence was not observed in the lungs of the rats treated with FITC-CSNPs. The fluorescence intensity in the liver peaked at 2 h in the FITC-CSNPs group, and it was significantly higher than that of the RBC-FITC-CSNPs group [25,29,49].

A similar result was observed for *in vivo* distribution of Cy7.5 in BALB/C mice. The results of the RBC-Cy7.5-CSNPs (Fig. 6D) revealed a strong fluorescence signal in the lungs 2–4 h post injection, followed by a gradual decrease in the signal. In contrast, Cy7.5-CSNPs resulted in fluorescence signals in the liver, but no evident fluorescence signals in the lungs. Mice were sacrificed at 4 h and 12 h post injection, and the main organs (heart, liver, spleen, lung, and kidney) were harvested and imaged with the imaging system. RBC-Cy7.5-CSNPs showed the strongest lung-targeting ability. Compared with the Cy7.5-CSNPs group, the fluorescence signal in the RBC-Cy7.5-CSNPs group was remarkably reduced in the liver and significantly increased in the lungs. Moreover, the fluorescence of Cy7.5 could still be observed in the lungs even 12 h after injection.

The lung is the only organ that receives more than 50% of the total cardiac blood output because of high distribution of vascular endothelium. In addition, blood elements were squeezed in the alveolar capillaries when passing through the air-blood barrier microcirculation, causing the carrier RBCs to deposit the NPs in the lungs, which gradually accumulates during cycling. Therefore, RBC-hitchhiking NPs not only possessed lung-targeting ability, but they were also able to avoid clearance by the RES. RBC-based delivery of NPs often has desirable properties. In contrast to the negatively charged NPs, positively charged CSNPs allow adhesion to the negatively charged RBCs. Consequently, RBC-hitchhiking could allow a significant and abundant accumulation of NPs in the lungs, prolonging *in vivo* circulation time of positively charged NPs.

3.6. Effect of RBC-hitchhiking on LPS-induced ALI

The therapeutic potential of RBC-hitchhiking on ALI/ARDS was evaluated using a rat model of LPS-induced ALI, which represents pulmonary capillary endothelial dysfunction and influx of destructive leukocytes, and resembles the cytokine storm scenario characterized by increased levels of inflammatory cytokines [8,37]. The experimental scheme is shown in Fig. 7A. Two pivotal cytokines (TNF-α and IL-6), which are closely related to an inflammatory response, were measured in the serum, revealing that low levels of these cytokines were present in the control group (without LPS). However, these two cytokines were significantly increased at 5 h after LPS treatment, thus inducing inflammation. The concentrations of TNF-α and IL-6 in the PBS group remained high up to 48 h post intravenous injection, showing significantly higher levels than those in the control and all treated groups. The concentrations of TNF-α and IL-6 in the three treated groups were decreased upon drug injection. Notably, levels of these two inflammatory factors in the group treated with RBC-MPSS-CSNPs were significantly lower than those in the groups treated with MPSS and MPSS-CSNPs (Fig. 7B and C). In addition, the levels of inflammatory cytokines in BALF revealed that the concentrations of TNF-α and IL-6 in all treatment groups were significantly lower than that after PBS treatment. Notably, the levels of inflammatory cytokines in the RBC-MPSS-CSNPs group were remarkably lower than those in the MPSS and MPSS-CSNPs groups (Fig. 8A and B).

Myeloperoxidase (MPO) activity, an indicator of polymorphonuclear-leukocyte (PMN) accumulation in the lungs, was determined. We observed a significant decrease in MPO level in BALF and in the lungs of RBC-MPSS-CSNPs treated rats than in those of the control groups, including the PBS, MPSS, and MPSS-CSNPs groups (Fig. 8C). As shown in Fig. 8D, LPS treatment led to a significant increase of PMNs count in BALF. The number of PMNs was significantly lower in the three treatment groups 48 h after administration than in the PBS group; the greatest decrease was observed in the RBC-MPSS-CSNPs group.

Signs of lung inflammation such as inflammatory cell infiltration, significant increase in PMNs count, and dramatically increased levels of inflammatory factors were evident in the rats after LPS treatment. All treatment groups (MPSS, MPSS-CSNPs, and RBC-MPSS-CSNPs) showed lower levels of TNF-α and IL-6 expression than did the non-treated group

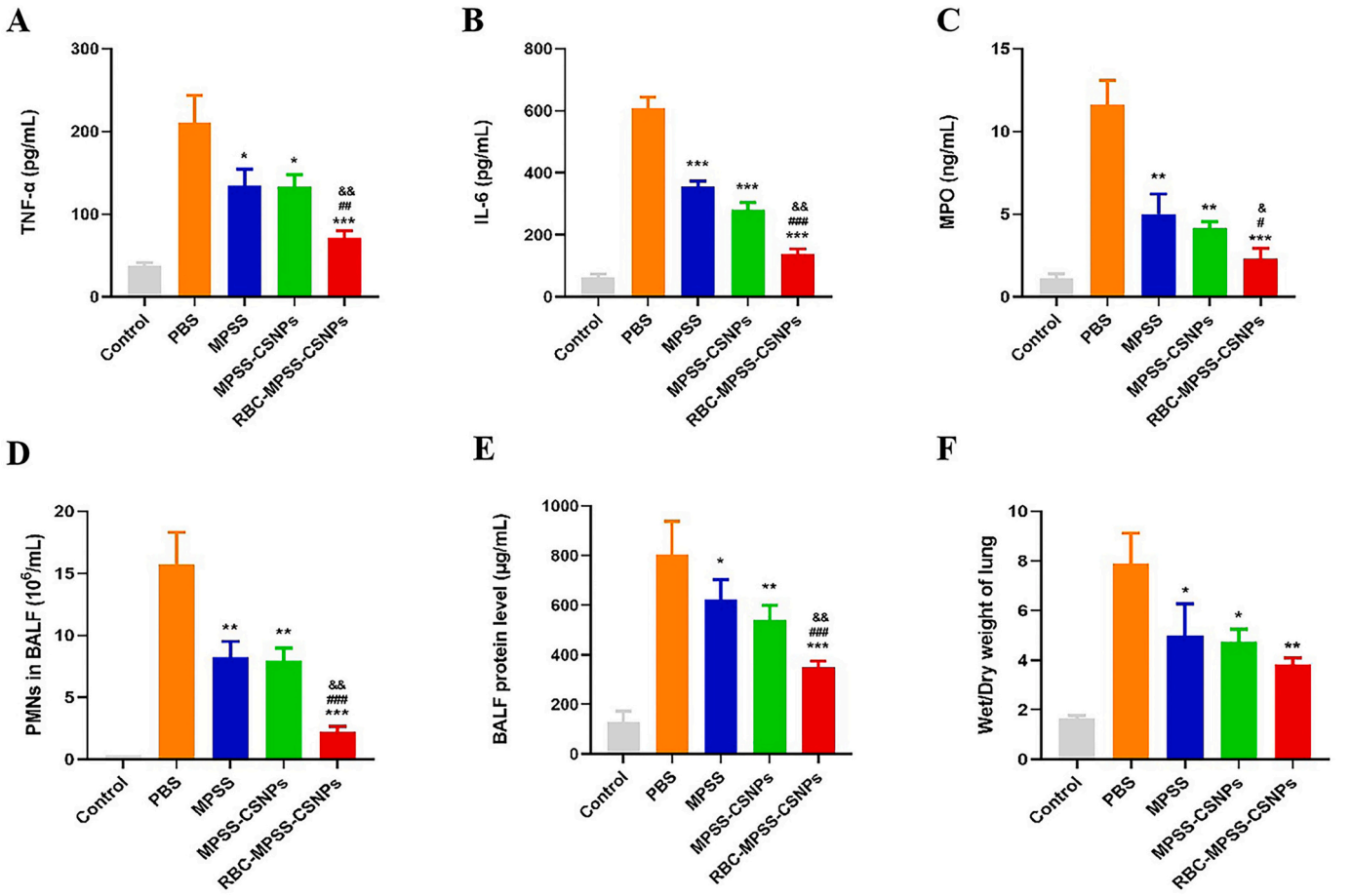

Fig. 8. The Bronchoalveolar lavage fluid (BALF) inflammatory cytokines levels reflect the level of inflammation. Expression of (A) TNF-α and (B) IL-6 in BALF. (C) MPO activity in BALF. (D) PMNs in BALF. (E)The concentrations of total protein in BALF (F) Wet to dry (W/D) lung weight ratios. Data represent mean ± SD ($n = 6$). $^{*}p < 0.05$, $^{**}p < 0.01$ $^{***}p < 0.001$ *vs* PBS; $^{\#}p < 0.05$, $^{\#\#}p < 0.01$ and $^{\#\#\#}p < 0.001$ *vs* MPSS; $^{\&}p < 0.05$, $^{\&\&}p < 0.01$ and $^{\&\&\&}p < 0.001$ *vs* MPSS-CSNPs.

(PBS group). Among all groups, the effect of treatment with RBC-MPSS-CSNPs was the most significant. This is attributed to the fact that during ALI, RBC-hitchhiking delivered MPSS-CSNPs to the pulmonary capillary endothelial cells, and the leukocytes lining the luminal capillary surface were the prominent target of the treatment [45]. Therefore, RBC-hitchhiking promoted abundant accumulation of MPSS-CSNPs in the lungs, resulting in a high concentration of MPSS to combat lung inflammation, consequently inhibiting the production of LPS-induced inflammatory cytokines and inflammatory mediators. RBC-MPSS-CSNPs suppressed the pro-inflammatory responses, thereby avoiding the more severe inflammatory response caused by exuberant increase in cytokine levels— the so-called cytokine storm.

During lung injury, protein-rich fluids leak due to the disruption of the alveolar-capillary membrane; therefore, concentration of the total protein in BALF was used as a marker of pulmonary damage [50]. The total protein in BALF of the PBS group was significantly higher than that of the control group (Fig. 8D). Moreover, the total protein concentration in BALF was significantly decreased, to different degrees, after administration of MPSS, MPSS-CSNPs, and RBC-MPSS-CSNPs, and a more dramatic decrease was observed in the RBC-MPSS-CSNPs group than in the other two treatment groups.

The increased capillary permeability may lead to lung edema, resulting in impaired gas exchange. Thus, hypoxia, an index of lung injury, was evaluated in accordance with the lung wet/dry weight ratio [51]. The results showed that the lung W/D weight ratio showed a four-fold increase after LPS treatment, compared with the control group. The lung W/D weight ratio was dramatically decreased in the MPSS, MPSS-CSNPs, and RBC-MPSS-CSNPs groups, suggesting a reduction in pulmonary edema. Moreover, the W/D weight ratio in the RBC-MPSS-CSNPs group was significantly lower than that in the other two treatment groups (Fig. 8E). Since the RBC-MPSS-CSNPs presumably blocked the production of inflammatory mediators through inhibition of cytokines, it could attenuate lung injury by decreasing lung edema to a greater extent.

The H&E staining of the lung tissue from each group of rats (Fig. 9E) revealed a significant pulmonary hemorrhage in the alveoli, bronchial wall thickening, and leukocyte infiltration in the PBS group. A significant histological improvement was observed in all treatment groups, but RBC-MPSS-CSNPs induced a more significant reduction of the alveolar hemorrhage, alveolar septal thickness, and infiltration of inflammatory cells than did the other treatment groups. Furthermore, in contrast to the PBS, MPSS, and MPSS-CSNPs groups, the RBC-MPSS-CSNPs group exhibited a more significant silencing effect on TNF-α and IL-6 at both mRNA (Fig. 9B and C) and protein levels (Fig. 9D and E).

To further investigate whether the inflammatory response caused excessive apoptosis, immunohistochemical staining was performed to detect the expression of IL-1β and caspase-1 in the lung tissue [52]. The results showed reduction in the expression of IL-1β and caspase-1 after treatment with MPSS, MPSS-CSNPs, and RBC-MPSS-CSNPs (Fig. 10). Notably, the mean densities of IL-1β and caspase-1 in the lung tissue of the RBC-MPSS-CSNPs group were significantly lower than in the other treatment groups, suggesting that apoptosis was reduced in the lung tissue (Fig. S1).

These results indicated that MPSS treatment favors the immune response activation. RBC-MPSS-CSNPs, with preferential accumulation in the lungs, were proven to further suppress systemic inflammatory

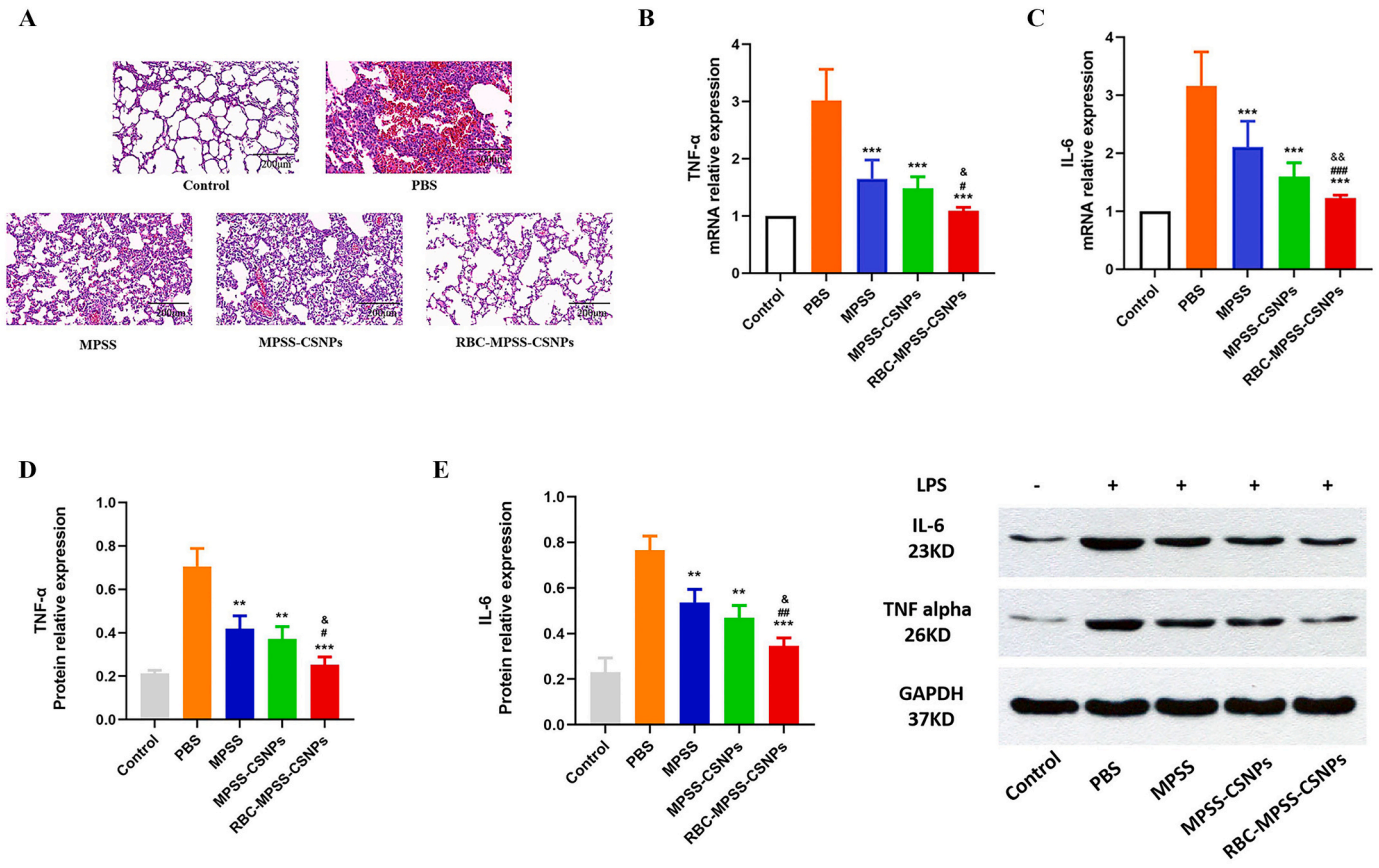

Fig. 9. (A) H&*E*-stained pathological sections of lung 48 h after the rat infected with LPS were treated with PBS, free MPSS, MPSS-CSNPs and RBC-MPSS-CSNPs, respectively. Scale bar: 200 μm. (B) TNF-α and (C) IL-6 mRNA expression levels of lung tissues harvested from the rat quantified by qRT-PCR. (mean ± SD, n = 6). Western blot detection (D) IL-6 and (E) TNF-α measured in lung tissues using GAPDH as reference protein. (mean ± SD, n = 6). *p < 0.05, **p < 0.01 ***p < 0.001 *vs* PBS; $^{\#}$p < 0.05, $^{\#\#}$p < 0.01 and $^{\#\#\#}$p < 0.001 *vs* MPSS; $^{\&}$p < 0.05, $^{\&\&}$p < 0.01 and $^{\&\&\&}$p < 0.001 *vs* MPSS-CSNPs.

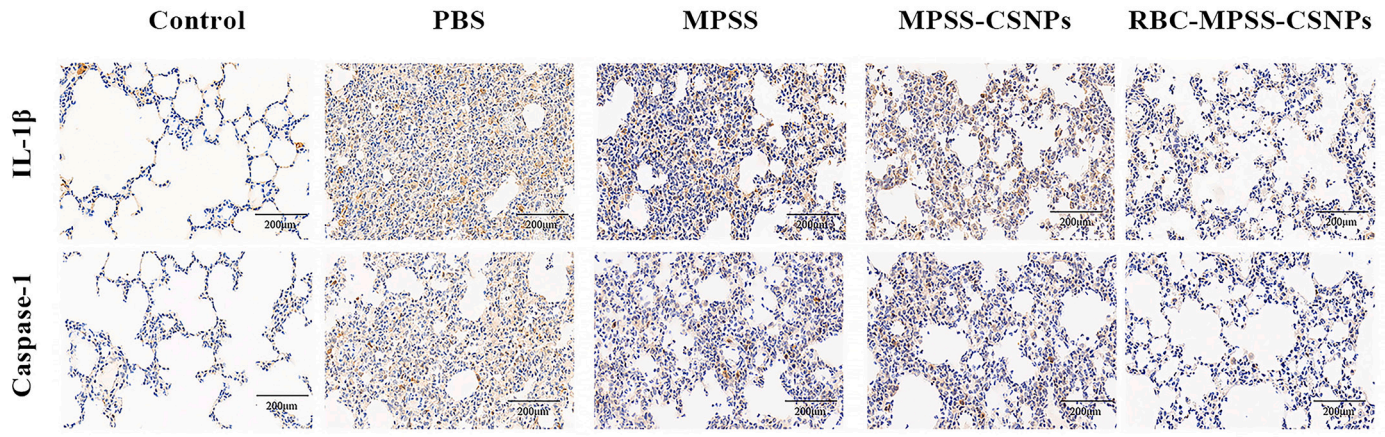

Fig. 10. Immunohistochemical (IHC) in the lung tissues (A) IHC staining for caspase 1 and IL-1β respectively. Scale bar: 200 μm.

responses in the lungs through downregulation of TNF-α and IL-6 expression and attenuation of systemic edema.

4. Conclusions

In the present study, RBC-MPSS-CSNPs were designed, prepared, and evaluated. The results of *in vivo* pharmacokinetic and distribution studies indicated that the RBC-MPSS-CSNPs could prolong the circulation time and improve lung targeting while avoiding RES clearance. Treatment with RBC-MPSS-CSNPs reduced the levels of TNF-α and IL-6 in rats and the expression of IL-1β and caspase-1 in the lung tissues, contributing to the reduction of inflammation and thereby alleviating lung injury. Although MPSS-CSNPs could sustain the drug release and extend the half-life of the drug, the MPSS-CSNPs were rapidly cleared by the liver and spleen, and this largely reduced their bioavailability. RBC-MPSS-CSNPs exploited the erythrocytes, which are the most abundant circulating cells in the blood. They are used to avoid RES clearance, prolong the circulation time of the NPs, and improve the targeting

ability of non-targeted particles to the lungs. Thus, RBC-hitchhiking could provide novel approach in the therapy of lung diseases such as chronic obstructive pulmonary disease, pulmonary hypertension, lung cancer, cystic fibrosis, asthma, and respiratory infectious diseases (including COVID-19).

Declaration of Competing Interest

The authors report no conflict of interest.

Acknowledgements

This study was supported by the National Science and Technologies Major Projects for "Major New Drugs Innovation and Development" (Grant No. 2018ZX09711003-008-001).

Appendix A. Supplementary data

Supplementary data to this article can be found online at https://doi.org/10.1016/j.jconrel.2021.12.018.

References

[1] L.Y.C. Chen, T.T.T. Quach, COVID-19 cytokine storm syndrome: a threshold concept, Lancet Microbe 2 (2) (2021) e49–e50.
[2] X. Yongzhi, COVID-19-associated cytokine storm syndrome and diagnostic principles: an old and new issue, Emerg. Microb. Infect. 10 (1) (2021) 266–276.
[3] J. Zhao, L. Wang, M. Schank, X. Dang, Z. Lu, D. Cao, S. Khanal, L.N. Nguyen, L.N. T. Nguyen, J. Zhang, Y. Zhang, J.L. Adkins, E.M. Baird, X.Y. Wu, S. Ning, M. E. Gazzar, J.P. Moorman, Z.Q. Yao, SARS-CoV-2 specific memory T cell epitopes identified in COVID-19-recovered subjects, Virus Res. 198508 (2021).
[4] M.N.J. Woodall, T. Masonou, K.M. Case, C.M. Smith, Human models for COVID-19 research, J. Physiol. 599 (18) (2021) 4255–4267.
[5] N. Teoh, G. Farrell, Statins as early therapy to mitigate COVID-19 (SARS-CoV-2)-associated ARDS and cytokine storm syndrome - time is of the essence, J. Clin. Transl. Res. 5 (5) (2020) 227–229.
[6] A. Bektas, S.H. Schurman, C. Franceschi, L. Ferrucci, A public health perspective of aging: do hyper-inflammatory syndromes such as COVID-19, SARS, ARDS, cytokine storm syndrome, and post-ICU syndrome accelerate short- and long-term inflammaging? Immun. Ageing 17 (2020) 23.
[7] E. Calvo-Aranda, I. Canamares-Orbis, M. Novella-Navarro, A. Martinez-Alcala, O. M. de la Ortega, I. Escobar-Rodriguez, F.M. Sanchez-Aranda, Correspondence on 'Historically controlled comparison of glucocorticoids with or without tocilizumab versus supportive care only in patients with COVID-19-associated cytokine storm syndrome: results of the CHIC study', Ann. Rheum. Dis. 79 (9) (2020) 1143–1151.
[8] R. Molinaro, A. Pasto, F. Taraballi, F. Giordano, J.A. Azzi, E. Tasciotti, C. Corbo, Biomimetic nanoparticles potentiate the anti-inflammatory properties of dexamethasone and reduce the cytokine storm syndrome: an additional weapon against COVID-19? Nanomater. (Basel) 10 (11) (2020).
[9] P. Hassanzadeh, Nanotheranostics against COVID-19: from multivalent to immune-targeted materials, J. Control. Release 328 (2020) 112–126.
[10] C. Chakraborty, A.R. Sharma, M. Bhattacharya, G. Sharma, S.S. Lee, G. Agoramoorthy, COVID-19: consider IL-6 receptor antagonist for the therapy of cytokine storm syndrome in SARS-CoV-2 infected patients, J. Med. Virol. 92 (11) (2020) 2260–2262.
[11] H.W. Yoo, J.I. Shin, D.K. Yon, S.W. Lee, COVID-19 morbidity and severity in patients with non-alcoholic fatty liver disease in South Korea: a nationwide cohort study, Clin. Gastroenterol. Hepatol. 21 (2021) 1542–3565.
[12] F.R. Formiga, R. Leblanc, J. de Souza Reboucas, L.P. Farias, R.N. de Oliveira, L. Pena, Ivermectin: an award-winning drug with expected antiviral activity against COVID-19, J. Control. Release 329 (2021) 758–761.
[13] S. Lu, Q. Zhou, L. Huang, Q. Shi, S. Zhao, Z. Wang, W. Li, Y. Tang, Y. Ma, X. Luo, T. Fukuoka, H.S. Ahn, M.S. Lee, Z. Luo, E. Liu, Y. Chen, C. Zhou, D. Peng, Effectiveness and safety of glucocorticoids to treat COVID-19: a rapid review and meta-analysis, Ann. Transl. Med. 8 (10) (2020) 627.
[14] G.G. Luetic, M.L. Menichini, O. Fernandez, Oral administration of methylprednisolone powder for intravenous injection dissolved in water to treat MS and NMOSD relapses during COVID-19 pandemic in a real-world setting, Mult. Scler. Relat. Disord. 54 (2021), 103148.
[15] E. Ricciotti, K. Laudanski, G.A. FitzGerald, Nonsteroidal anti-inflammatory drugs and glucocorticoids in COVID-19, Adv. Biol. Regul. 81 (2021), 100818.
[16] S. Ro, N. Nishimura, R. Imai, Y. Tomishima, C. So, M. Murakami, K. Okafuji, A. Kitamura, T. Jinta, T. Tamura, Identification of patients with COVID-19 who are optimal for methylprednisolone pulse therapy, Multidiscip. Respir. Med. 16 (1) (2021) 781.
[17] V. Brar, G. Kaur, Preparation of chitosan okra nanoparticles: optimization and evaluation as Mucoadhesive drug delivery system, Pharm. Nanotechnol. 6 (3) (2018) 180–191.
[18] C. Canepa, J.C. Imperiale, C.A. Berini, M. Lewicki, A. Sosnik, M.M. Biglione, Development of a drug delivery system based on chitosan nanoparticles for Oral Administration of Interferon-alpha, Biomacromolecules 18 (10) (2017) 3302–3309.
[19] F. Fenaroli, D. Westmoreland, J. Benjaminsen, T. Kolstad, F.M. Skjeldal, A. H. Meijer, M. van der Vaart, L. Ulanova, N. Roos, B. Nystrom, J. Hildahl, G. Griffiths, Nanoparticles as drug delivery system against tuberculosis in zebrafish embryos: direct visualization and treatment, ACS Nano 8 (7) (2014) 7014–7026.
[20] S. Ahmad, M.A.I. Al-Hatamleh, R. Mohamud, Targeting immunosuppressor cells with nanoparticles in autoimmunity: how far have we come to? Cell. Immunol. 368 (2021), 104412.
[21] T. Yu, A. Malugin, H. Ghandehari, Impact of silica nanoparticle design on cellular toxicity and hemolytic activity, ACS Nano 5 (7) (2011) 5717–5728.
[22] F. Alexis, E. Pridgen, L.K. Molnar, O.C. Farokhzad, Factors affecting the clearance and biodistribution of polymeric nanoparticles, Mol. Pharm. 5 (4) (2008) 505–515.
[23] E. Chambers, S. Mitragotri, Prolonged circulation of large polymeric nanoparticles by non-covalent adsorption on erythrocytes, J. Control. Release 100 (1) (2004) 111–119.
[24] A.C. Anselmo, V. Gupta, B.J. Zern, D. Pan, M. Zakrewsky, V. Muzykantov, S. Mitragotri, Delivering nanoparticles to lungs while avoiding liver and spleen through adsorption on red blood cells, ACS Nano 7 (12) (2013) 11129–11137.
[25] J.S. Brenner, D.C. Pan, J.W. Myerson, O.A. Marcos-Contreras, C.H. Villa, P. Patel, H. Hekierski, S. Chatterjee, J.Q. Tao, H. Parhiz, K. Bhamidipati, T.G. Uhler, E. D. Hood, R.Y. Kiseleva, V.S. Shuvaev, T. Shuvaeva, M. Khoshnejad, I. Johnston, J. V. Gregory, J. Lahann, T. Wang, E. Cantu, W.M. Armstead, S. Mitragotri, V. Muzykantov, Red blood cell-hitchhiking boosts delivery of nanocarriers to chosen organs by orders of magnitude, Nat. Commun. 9 (1) (2018) 2684.
[26] X. Han, C. Wang, Z. Liu, Red blood cells as smart delivery systems, Bioconjug. Chem. 29 (4) (2018) 852–860.
[27] G.I. Harisa, M.F. Ibrahim, F. Alanazi, G.A. Shazly, Engineering erythrocytes as a novel carrier for the targeted delivery of the anticancer drug paclitaxel, Saudi Pharm. J. 22 (3) (2014) 223–230.
[28] H. Ye, Z. Shen, M. Wei, Y. Li, Red blood cell hitchhiking enhances the accumulation of nano- and micro-particles in the constriction of a stenosed microvessel, Soft Matter 17 (1) (2021) 40–56.
[29] I.V. Zelepukin, A.V. Yaremenko, V.O. Shipunova, A.V. Babenyshev, I.V. Balalaeva, P.I. Nikitin, S.M. Deyev, M.P. Nikitin, Nanoparticle-based drug delivery via RBC-hitchhiking for the inhibition of lung metastases growth, Nanoscale 11 (4) (2019) 1636–1646.
[30] N.C. Silva, S. Silva, B. Sarmento, M. Pintado, Chitosan nanoparticles for daptomycin delivery in ocular treatment of bacterial endophthalmitis, Drug Deliv. 22 (7) (2015) 885–893.
[31] Y. Wang, C. Zhou, Y. Ding, M. Liu, Z. Tai, Q. Jin, Y. Yang, Z. Li, M. Yang, W. Gong, C. Gao, Red blood cell-hitchhiking chitosan nanoparticles for prolonged blood circulation time of vitamin K1, Int. J. Pharm. 592 (2021), 120084.
[32] A. Nasti, N.M. Zaki, P. de Leonardis, S. Ungphaiboon, P. Sansongsak, M.G. Rimoli, N. Tirelli, Chitosan/TPP and chitosan/TPP-hyaluronic acid nanoparticles: systematic optimisation of the preparative process and preliminary biological evaluation, Pharm. Res. 26 (8) (2009) 1918–1930.
[33] W. Fan, W. Yan, Z. Xu, H. Ni, Erythrocytes load of low molecular weight chitosan nanoparticles as a potential vascular drug delivery system, Colloids Surf. B: Biointerfaces 95 (2012) 258–265.
[34] X. Zhang, M. Qiu, P. Guo, Y. Lian, E. Xu, J. Su, Autologous red blood cell delivery of betamethasone phosphate sodium for long anti-inflammation, Pharmaceutics 10 (4) (2018).
[35] Y. Feng, Q. Liu, Y. Li, Y. Han, M. Liang, H. Wang, Q. Yao, Y. Wang, M. Yang, Z. Li, W. Gong, Y. Yang, C. Gao, Cell relay-delivery improves targeting and therapeutic efficacy in tumors, Bioact. Mater. 6 (6) (2021) 1528–1540.
[36] Y. Han, C. Gao, H. Wang, J. Sun, M. Liang, Y. Feng, Q. Liu, S. Fu, L. Cui, C. Gao, Y. Li, Y. Yang, B. Sun, Macrophage membrane-coated nanocarriers co-modified by RVG29 and TPP improve brain neuronal mitochondria-targeting and therapeutic efficacy in Alzheimer's disease mice, Bioact. Mater. 6 (2) (2021) 529–542.
[37] Y. Wang, L. Ding, Z. Li, G. Chen, M. Sun, D. Oupicky, Treatment of acute lung injury and early- and late-stage pulmonary fibrosis with combination emulsion siRNA polyplexes, J. Control. Release 314 (2019) 12–24.
[38] A.C. Anselmo, S. Mitragotri, Cell-mediated delivery of nanoparticles: taking advantage of circulatory cells to target nanoparticles, J. Control. Release 190 (2014) 531–541.
[39] P.I.P. Soares, A.I. Sousa, J.C. Silva, I.M.M. Ferreira, C.M.M. Novo, J.P. Borges, Chitosan-based nanoparticles as drug delivery systems for doxorubicin: optimization and modelling, Carbohydr. Polym. 147 (2016) 304–312.
[40] D.Y. Arifin, L.Y. Lee, C.H. Wang, Mathematical modeling and simulation of drug release from microspheres: implications to drug delivery systems, Adv. Drug Deliv. Rev. 58 (12–13) (2006) 1274–1325.
[41] E.S. Kim, D.Y. Kim, J.S. Lee, H.G. Lee, Quercetin delivery characteristics of chitosan nanoparticles prepared with different molecular weight polyanion cross-linkers, Carbohydr. Polym. 267 (2021), 118157.
[42] M. Magnani, L. Rossi, A. Casabianca, A. Fraternale, G. Schiavano, G. Brandi, F. Mannello, G. Piedimonte, Red blood cells as advanced drug delivery systems for antiviral nucleoside analogues, Adv. Exp. Med. Biol. 326 (1992) 239–245.
[43] M.I. Kamalov, T. Dang, N.V. Petrova, A.V. Laikov, D. Luong, R.A. Akhmadishina, A. N. Lukashkin, T.I. Abdullin, Self-assembled nanoformulation of methylprednisolone succinate with carboxylated block copolymer for local glucocorticoid therapy, Colloids Surf. B: Biointerfaces 164 (2018) 78–88.

[44] A.N. Kong, G.L. Jungbluth, M.T. Pasko, T.R. Beam, W.J. Jusko, Pharmacokinetics of methylprednisolone sodium succinate and methylprednisolone in patients undergoing cardiopulmonary bypass, Pharmacotherapy 10 (1) (1990) 29–34.
[45] N. Bertrand, P. Grenier, M. Mahmoudi, E.M. Lima, E.A. Appel, F. Dormont, J. M. Lim, R. Karnik, R. Langer, O.C. Farokhzad, Mechanistic understanding of in vivo protein corona formation on polymeric nanoparticles and impact on pharmacokinetics, Nat. Commun. 8 (1) (2017) 777.
[46] P.M. Glassman, C.H. Villa, A. Ukidve, Z. Zhao, P. Smith, S. Mitragotri, A.J. Russell, J.S. Brenner, V.R. Muzykantov, Vascular drug delivery using carrier red blood cells: focus on RBC surface loading and pharmacokinetics, Pharmaceutics 12 (5) (2020).
[47] J.S. Brenner, S. Mitragotri, V.R. Muzykantov, Red blood cell hitchhiking: a novel approach for vascular delivery of Nanocarriers, Annu. Rev. Biomed. Eng. 23 (2021) 225–248.
[48] C.H. Villa, A.C. Anselmo, S. Mitragotri, V. Muzykantov, Red blood cells: supercarriers for drugs, biologicals, and nanoparticles and inspiration for advanced delivery systems, Adv. Drug Deliv. Rev. 106 (Pt A) (2016) 88–103.
[49] A.C. Anselmo, S. Kumar, V. Gupta, A.M. Pearce, A. Ragusa, V. Muzykantov, S. Mitragotri, Exploiting shape, cellular-hitchhiking and antibodies to target nanoparticles to lung endothelium: synergy between physical, chemical and biological approaches, Biomaterials 68 (2015) 1–8.
[50] H.A. Kim, J.H. Park, S. Lee, J.S. Choi, T. Rhim, M. Lee, Combined delivery of dexamethasone and plasmid DNA in an animal model of LPS-induced acute lung injury, J. Control. Release 156 (1) (2011) 60–69.
[51] K. Wang, Y. Lei, D. Xia, P. Xu, T. Zhu, Z. Jiang, Y. Ma, Neutrophil membranes coated, antibiotic agent loaded nanoparticles targeting to the lung inflammation, Colloids Surf. B: Biointerfaces 188 (2020), 110755.
[52] H. Jin, Z. Zhao, Q. Lan, H. Zhou, Z. Mai, Y. Wang, X. Ding, W. Zhang, J. Pi, C. E. Evans, X. Liu, Nasal delivery of hesperidin/chitosan nanoparticles suppresses cytokine storm syndrome in a mouse model of acute lung injury, Front. Pharmacol. 11 (2020), 592238.